Article

Investigating the Temporal and Spatial Dynamics of Human Development Index: A Comparative Study on Countries and Regions in the Eastern Hemisphere from the Perspective of Evolution

Hanwei Liang [1,2,*], Na Li [1], Ji Han [3,4], Xin Bian [1], Huaixia Xia [1] and Liang Dong [5]

1 Collaborative Innovation Center on Forecast and Evaluation of Meteorological Disasters (CIC-FEMD), School of Geographical Sciences, Nanjing University of Information Science and Technology (NUIST), Nanjing 210044, China; li.na@nuist.edu.cn (N.L.); Bianxin@nuist.edu.cn (X.B.); xia.huaixia@nuist.edu.cn (H.X.)
2 Key Laboratory of Coastal Zone Exploitation and Protection, Ministry of Natural Resources, Nanjing 210024, China
3 Shanghai Key Lab for Urban Ecological Processes and Eco-Restoration, School of Ecological and Environmental Sciences, East China Normal University, Dongchuan Rd. 500, Shanghai 200241, China; jhan@re.ecnu.edu.cn
4 Institute of Eco-Chongming, 3663 N. Zhongshan Rd., Shanghai 200062, China
5 Department of Public Policy, and School of Energy and Environment, City University of Hong Kong, Hong Kong 999077, China; liadong@cityu.edu.hk
* Correspondence: liang.hanwei@nuist.edu.cn

Abstract: The Human Development Index (HDI) is a prevailing indicator to present the status and trend of sustainability of nations, hereby offers a valuable measurement on the Sustainable Development Goals (SDGs). Revealing the dynamics of the HDI of the Eastern Hemisphere countries is vital for measurement and evaluation of the human development process and revealing the spatial disparities and evolutionary characteristics of human development. However, the statistical data-based HDI, which is currently widely applied, has defects in terms of data availability and inconsistent statistical caliber. To tackle such an existing gap, we applied nighttime lights (NTL) data to reconstruct new HDI indicators named HDI_{NTL} and quantify the HDI_{NTL} at multispatial scales of Eastern Hemisphere countries during 1992–2013. Results showed that South Central Asia countries had the smallest discrepancies in HDI_{NTL}, while the largest was found in North Africa. The national-level HDI_{NTL} values in the Eastern Hemisphere ranged between 0.138 and 0.947 during 1992–2013. At the subnational scale, the distribution pattern of HDI_{NTL} was spatially clustered based on the results of spatial autocorrelation analysis. The evolutionary trajectory of subnational level HDI_{NTL} exhibited a decreasing and then increasing trend along the northwest to the southeast direction of Eastern Hemisphere. At the pixel scale, 93.52% of the grids showed an increasing trend in HDI_{NTL}, especially in the urban agglomerations of China and India. These results are essential for the ever-improvement of policy making to reduce HDI's regional disparity and promote the continuous development of humankind's living qualities. This study offers an improved HDI accounting method. It expects to extend the channel of HDI application, e.g., potential integration with environmental, physical, and socioeconomic data where the NTL data could present as well.

Keywords: human development index; nighttime lights; Eastern Hemisphere; spatial disparity; evolutionary trajectory

1. Introduction

The international community and countries have widely adopted the Sustainable Development Goals (SDGs) set by the United Nations General Assembly in 2015. The 17 SDGs, including No Poverty, Good Health and Well-Being, Quality Education, Decent

Work and Economic Growth, and Reduced Inequalities, provide us with a joint program and agenda to address social, economic, and environmental challenges. The achievement of these goals is closely linked to human socioeconomic activities between countries and regions. The Eastern Hemisphere, composed of Africa–Eurasia (Africa and Eurasia) and Australia, is also the countries and regions involved in the Belt and Road Initiative, whose human development processes will significantly impact global economic growth, industrial structure, and resource allocation [1]. Moreover, since Eastern Hemisphere regions and countries differ significantly in cultural background, medical level, economic development, population base, and education level, assessing the current human and economic development of these regions and countries is important to reduce the differences in human development in the region and thus achieve sustainable development.

The Human Development Index (HDI) was first proposed by the United Nations Development Programme (UNDP) in 1990 [2], aiming to solve the problem of GDP as a development indicator lacking attention to the quality of development and ignoring the fairness of individual opportunities in society [3]. It is one of the most widely used indicators to reflect socioeconomic development status [4,5]. The HDI measures social and economic development from a multidimensional perspective, covering information on three dimensions: healthy living, educational attainment, and standard of living [6]. These three subdimensional indicators are directly related to economic development, social progress, and human well-being [7,8]. Thus, evaluating HDI within a given geographic area is important for policy formulation, planning, implementation, and resource allocation [9,10]. For example, Sanusi [11] used the HDI as an essential proxy to measure poverty among urban households in Minna and Nigeria. Tian et al. [12] assessed the status of human well-being in China's Poyang Lake region based on the Human Development Index and spatial data indicators. Wang et al. [13] used HDI to analyze the relationship between energy and economic growth in Pakistan's human development process.

However, the commonly available HDI are mainly provided at the national level by large institutions such as UNDP and cannot reflect the spatial variability of human development within countries, especially at subnational scales and pixel scales [14]. Additionally, in the process of calculating the income index of HDI, direct comparison of economic development differences between countries and subnational units may not be reasonable due to possible inconsistencies in the statistical caliber of economic statistics in different countries [15]. Besides, the lack of data at spatial scales finer than national or provincial levels, particularly for social metrics, poses a major limitation to quantifying human well-being [16]. Therefore, we need to find suitable data to accurately assess and quantify human development processes within countries, both temporally and spatially.

Nighttime light data provides a reliable data source to capture the spatial disparities of economic development within countries [15,17]. As a supplement to the statistical database-based methods, the availability of nighttime lights (NTL) remote sensing data provides a novel option to study the status of socioeconomic variables that are difficult to determine at fine spatial scales, such as population [18–20], gross domestic product [21–24], electricity consumption [25,26], carbon emissions [27], and urban mineral stock [28,29]. Many existing studies show that NTL is closely related to economic activities and has the advantages of independence, objectivity, efficiency, and spatiotemporal continuity [30–32]. For instance, Gao et al. [33] pointed out that nighttime lights remote sensing imagery plays an essential role in monitoring socioeconomic changes in Eastern Hemisphere regions. Elvidge et al. [34] developed a nighttime lights development index (NLDI) based on NTL data and population density data, which drew on the Gini index's formula form and measured the inequality of human development from a global scale. Although previous studies have shown that nighttime lights brightness can be a good proxy for socioeconomic variables such as GDP under certain conditions [35–37], it is still unclear whether it can accurately characterize the human development status of Eastern Hemisphere and finely quantify the spatial–temporal patterns of HDI at multispatial scales.

However, few studies have focused on the linear relationship between GNP and NTL at the subnational level and use of NTL data to construct human development indicators based on this relationship to further analyze the spatial disparity and variability of HDI within countries or regions. Therefore, this study aims to propose NTL-based HDI indicators (HDI_{NTL}) to reveal the spatial–temporal evolution patterns of human development in 143 countries and regions in the Eastern Hemisphere during 1992–2013, and to provide valuable information for the sustainable human development measurement.

The research includes the following three aspects. (1) Establishing the national, subnational, and gridded level HDI_{NTL} databases based on NTL data can compensate for the traditional HDI limitations calculated based on statistical data. (2) Revealing the spatial disparity and clustering features of HDI_{NTL} at multispatial scales. (3) Quantify the development level, development type, and other evolutionary characteristics of HDI_{NTL} in the Eastern Hemisphere. The remainder of the paper is organized as follows: after this introductory section, Section 2 introduces the research area and data, as well as presents the methods, Section 3 presents the analytical results and discussions, and Section 4 draws conclusions and policy implications (Figure 1).
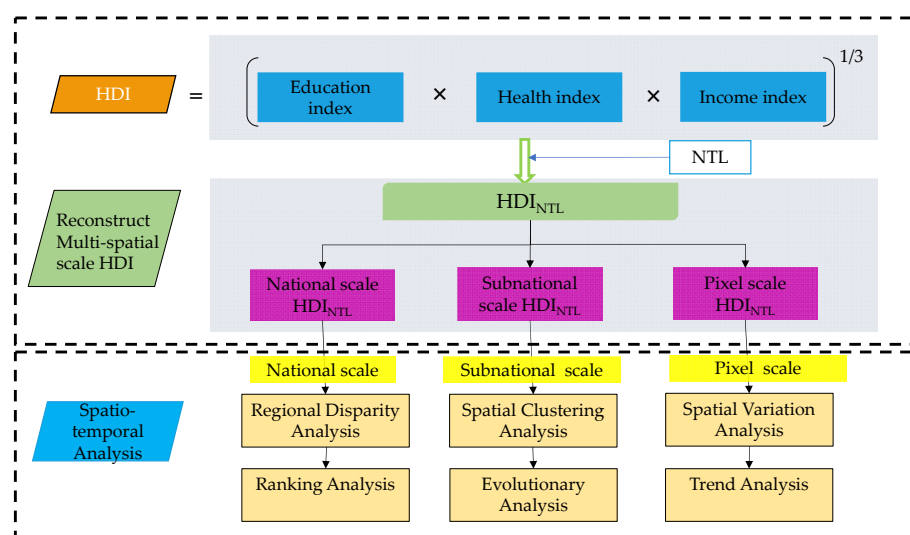

**Figure 1.** Theoretical framework.

2. Data and Methods

2.1. Study Area

According to the Annual Report on Remote Sensing Monitoring of Global Ecosystem and Environment released by the National Remote Sensing Center of China (GEOARC, 2017) [38] and the research of Herrmann and Mohr [39], we divided 143 Eastern Hemisphere countries and regions into 10 regions, namely Russia, West Asia, Central Asia, East Asia, South Asia, Europe, Oceania, Southeast Asia, North Africa, and Sub-Saharan Africa (Table 1 and Figure 2). One end of the Eastern Hemisphere is the vibrant East Asian economic circle; the other is the developed European economies, encompassing countries with huge economic development potential.

Table 1. Grouping of the Eastern Hemisphere countries.

Region	Countries
Russia	Russian Federation
West Asia	Armenia, Azerbaijan, Cyprus, Georgia, Iran, Iraq, Israel, Jordan, Kuwait, Lebanon, Oman, Palestine, Qatar, Saudi Arabia, Syria, Turkey, United Arab Emirates, Yemen
Central Asia	Kazakhstan, Kyrgyzstan, Tajikistan, Turkmenistan, Uzbekistan
East Asia	China, Japan, South Korea, Mongolia
South Asia	Afghanistan, Bangladesh, Bhutan, India, Nepal, Pakistan, Sri Lanka
Europe	Albania, Andorra, Austria, Belarus, Belgium, Bosnia and Herzegovina, Bulgaria, Croatia, Czech Republic, Denmark, Estonia, Finland, France, Germany, Greece, Hungary, Iceland, Ireland, Italy, Latvia, Liechtenstein, Lithuania, Luxembourg, Moldova, Monte Negro, Netherlands, North Macedonia, Norway, Poland, Portugal, Romania, Serbia, Slovakia, Slovenia, Spain, Sweden, Switzerland, Ukraine, United Kingdom
Oceania	Australia, New Zealand, Papua New Guinea, Solomon Islands, Vanuatu
Southeast Asia	Brunei Darussalam, Cambodia, Indonesia, Lao, Malaysia, Myanmar, Philippines, Singapore, Thailand, Timor-Leste, Vietnam
North Africa	Algeria, Burkina Faso, Chad, Djibouti, Egypt, Eritrea, Ethiopia, Libya, Mali, Mauritania, Morocco, Niger, Somalia, Sudan, Tunisia
Sub-Saharan Africa	Angola, Benin, Botswana, Burundi, Cameroon, Cape Verde, Central African Republic CAR, Comoros, Congo Brazzaville, Congo Democratic Republic, Cote d'Ivoire, Equatorial Guinea, eSwatini, Gabon, Gambia, Ghana, Guinea, Guinea Bissau, Kenya, Lesotho, Liberia, Madagascar, Malawi, Mauritius, Mozambique, Namibia, Nigeria, Rwanda, Sao Tome and Principe, Senegal, Sierra Leone, South Africa, South Sudan, Tanzania, Togo, Uganda, Zambia, Zimbabwe
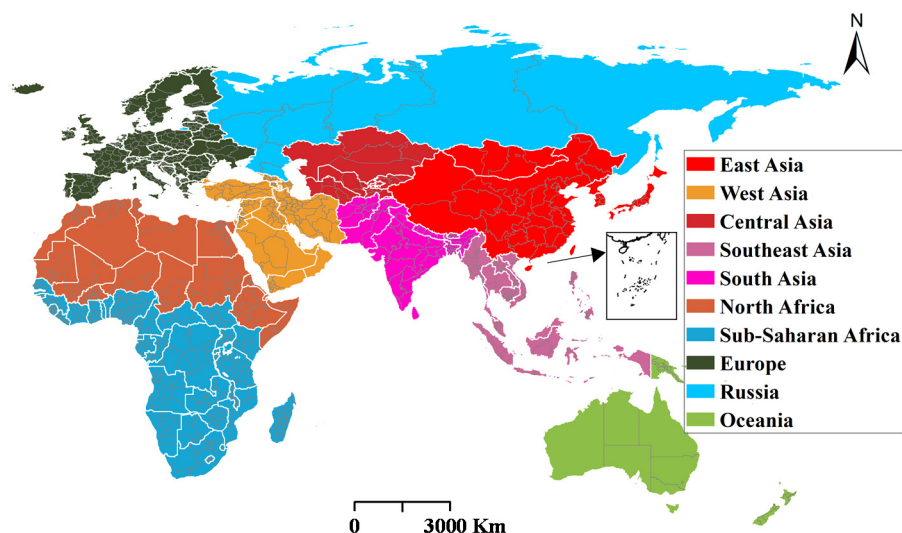
Figure 2. Spatial distribution of countries and regions in the Eastern Hemisphere.

2.2. Data and Preprocessing

The data used in this study include socioeconomic statistics data, population data, and satellite data (Table 2). We acquired the national and subnational socioeconomic statistics data (i.e., life expectancy at birth, mean years of schooling, expected years of schooling, gross national product (GNP), population) from the World Bank (https://data.worldbank.org.cn/, accessed on 14 June 2021) and publicly available datasets published by Smits and Permanyer [40]. Two population datasets were used to generate the time-series gridded maps of GNP per capita. One is HYDE 3.1 Population Dataset released by Klein Goldewijk et al. [41], its time coverage is 1992–1999, and spatial resolution is 5 arc-min (10 km at equator); another one is LandScan™ Global Popula-

tion Database developed by the Department of Energy's Oak Ridge National Laboratory (ORNL) (https://landscan.ornl.gov/, accessed on 14 June 2021), its time coverage is from 2000 onwards, and spatial resolution is 30 arc-sec (1 km at equator). To generate uniform resolution of population data, we allocated the population density proportionally in each 10×10 km grid of HYDE 3.1 Population Dataset into 100 1×1 km grids. Then all the HYDE 3.1 Population Dataset during 1992–1999 were resampled and had the same spatial resolution as ORNL's LandScan Population Database.

Table 2. Calculation data and source of Human Development Index (HDI_{NTL}).

Category	Remarks	Source
Socioeconomic statistics data	Life expectancy at birth Mean years of schooling Expected years of schooling Gross national product (GNP) Population Reported HDI	The national level data is provided by the UNDP (http://hdr.undp.org/en/data/, accessed on 14 June 2021) at National, 1992–2013; The subnational level data is downloaded from the Subnational Human Development Database [40], 1992–2013.
Gridded population data	5 arc-min (10 km at equator) 30 arc-sec (1 km at equator)	HYDE 3.1 Population Dataset [41], 1992–1999; Department of Energy's Oak Ridge National Laboratory (ORNL) (https://landscan.ornl.gov/, accessed on 14 June 2021), 2000–2013.
Nighttime lights data	The DMSP-OLS NTL product $(1 \times 1$ km)	NOAA/NGDC (http://ngdc.noaa.gov/eog/, accessed on 14 June 2021), 1992–2013.

Defense Meteorological Satellite Program's Operational Line Scan System (DMSP-OLS) Nighttime Lights Time-Series Product (version 4) is provided by the National Oceanic and Atmospheric Administration's National Geophysical Data Center (NOAA/NGDC) (http://ngdc.noaa.gov/eog/, accessed on 14 June 2021). Since this DMSP-OLS NTL product is obtained by multiple sensors without radiometric calibration, several preprocessing procedures (e.g., inter-calibration, intra-annual composition, and interannual series correction) are needed before comparing the pixel values in the individual year or compiling the comparable time series NTL data. Here, we referred to the previous study conducted by Elvidge et al. [42] to generate the time-series NTL data. The preprocessing procedures are briefly described: First, remove the gas flares captured by sensors from NTL satellite images. Then the F12 (1999) image of Sicily was used as the reference data, and the images obtained by individual satellites in other different years were adjusted by introducing quadratic regression models. Finally, the total digital number (DN) of lit pixels in each geographic boundary (i.e., national, subnational units) in the Eastern Hemisphere was summarized for building regression models with the income indicators. The quadratic regression model used in the second preprocessing step is as follows:

$$DN_{adjusted} = a \times DN^2 + b \times DN + c \tag{1}$$

where DN is the digital number of pixels before adjusted; $DN_{adjusted}$ is the adjusted digital number of pixels; a, b, and c are the coefficients of the second-order regression models, and the parameters of models are shown in Table S1 of supplementary material.

2.3. Methods

2.3.1. NTL-Based Human Development Indexes (HDI$_{NTL}$)

HDI$_{NTL}$ is a catch-all for the national, subnational, and gridded levels of human development indexes reconstructed using nighttime lights. The process of calculating HDI$_{NTL}$ is similar to the HDI released by UNDP [2]. The HDI of UNDP is a geometric mean of three-dimensional indices: Health Index, Education Index, and Income Index. The Income Index is a logarithmic form of GNP per capita. Here, we use the NTL data as a proxy for GNP to reconstruct the Income Index, and then propose the HDI$_{NTL}$. It comprises three-dimensional indices: Health Index, Education Index, and NTL Index. The NTL index is measured by the DN$_{adjusted}$ of lit NTL pixels in each geographic boundary (i.e., national, subnational units) in the Eastern Hemisphere. The calculating formula and max/min values of the Health Index and Education Index are consistent with UNDP [2]'s study at the national scale and Smits and Permanyer [40]'s study at the subnational scale. The calculation procedure of HDI$_{NTL}$ is as follows:

$$HDI^k_{NTL} = \sqrt[3]{I^k_{Health} \times I^k_{Education} \times I^k_{NTL}} \tag{2}$$

$$I^k_{NTL} = \frac{\ln NTL^k_{capita} - \min(\ln NTL^k_{capita})}{\max(\ln NTL^k_{capita}) - \min(\ln NTL^k_{capita})} \tag{3}$$

$$NTL^k_{capita} = \sum_{i=1}^{n} DN^k_{adjusted} / P^k \tag{4}$$

where HDI^k_{NTL} refers to the estimated HDI value of national or subnational unit k; I^k_{Health}, $I^k_{Education}$, and I^k_{NTL} are representative of Health Index, Education Index, and NTL Index of national or subnational unit k, respectively; NTL^k_{capita} refers to the total light brightness per capita of national or subnational unit k; $\min/\max(\ln NTL^k_{capita})$ refers to the upper/lower bound for the NTL^k_{capita} values in all national or subnational units in the Eastern Hemisphere during 1992–2013; $DN^k_{adjusted}$ is the adjusted digital number of lit pixels i within national or subnational unit k, and its value is greater than zero; P^k refers to the population size of national or subnational unit k.

We calculated the national HDI$_{NTL}$ (NHDI$_{NTL}$) and subnational HDI$_{NTL}$ (SHDI$_{NTL}$) based on the above formula. To maintain consistency between NHDI$_{NTL}$ and SHDI$_{NTL}$, we did not use SHDI$_{NTL}$ directly but introduced a scale factor to obtain the adjusted SHDI$_{NTL}$ for final use. The scale factor is determined by computing the ratio between the SHDI$_{NTL}$ and the population-weighted average of SHDI$_{NTL}$ for each subnational unit in the Eastern Hemisphere. The corresponding equation is presented as follows:

$$SHDI^{i,j}_{adjusted} = NHDI^i_{NTL} \times r^{i,j} \tag{5}$$

$$r^{i,j} = SHDI^{i,j}_{NTL} / \frac{\sum_{j=1}^{n} \left(SHDI^{i,j}_{NTL} \times P^{i,j} \right)}{\sum_{j=1}^{n} P^{i,j}} \tag{6}$$

where $SHDI^{i,j}_{adjusted}$ and $SHDI^{i,j}_{NTL}$ refer to the adjusted and estimated HDI$_{NTL}$ value of subnational unit j within nation i; $NHDI^i_{NTL}$ refers to the HDI$_{NTL}$ of nation j; $r^{i,j}$ refers to the scale factor for each subnational unit j within nation i; $P^{i,j}$ refers to the population size of subnational unit j within nation i.

Similarly, we introduced another scale factor to calculate the gridded level of HDI$_{NTL}$ (PHDI$_{NTL}$) based on SHDI$_{adjusted}$. The scale factor is determined by computing the ratio between the DN$_{adjusted}$ and the population-weighted average of DN$_{adjusted}$ for each gridded

unit (see Equation (5)). The final $PHDI_{NTL}$ ($PHDI_{adjusted}$) was calculated by multiplying the ratio with the $SHDI_{adjusted}$ (Equation (6)). Thus, based on the $NHDI_{NTL}$, $SHDI_{adjusted}$, and $PHDI_{adjusted}$ obtained in the above steps, we integrated the time-series of HDI_{NTL} at the nation, subnational, and pixel scale. It is worth noting that if not otherwise specified, the $SHDI_{NTL}$ and $PHDI_{NTL}$ refer to adjusted subnational and pixel scale HDI values, respectively.

Note that this study adopted the methods proposed by Kummu et al. (2018) to adjust HDI_{NTL} at the provincial and pixel levels by introducing different scale factors. This is because there was no significant relation between population proportion versus health index, education index, and NTL index at the subnational scale (data not shown). At pixel scale, we hypothesized that these relationships were also valid. Therefore, the population proportion was used to calculate the gridded level of HDI_{NTL}.

2.3.2. Spatial Autocorrelation Analysis

Spatial autocorrelation analysis is a powerful tool for analyzing spatial variability and relativity, which can reasonably reveal the geospatial distribution pattern of HDI_{NTL}. Here, we first applied the widely adopted Global Moran's *I* index to explore the spatial aggregation of $SHDI_{NTL}$. Then, we used hotspot analysis to clarify the hot/cold spatial aggregation areas of $SHDI_{NTL}$ in the Eastern Hemisphere. I_{global} and G_i^* (Getis-Ord G_i^* statistic) are the statistics used in Global Moran's *I* index and hotspot analysis, respectively [43–45]. The general form of I_{global} and G_i^* was given by:

$$I_{global} = \frac{n \sum\limits_{i=1}^{n} \sum\limits_{j=1}^{n} w_{ij}(X_i - \overline{X})(X_j - \overline{X})}{\sum\limits_{i=1}^{n} \sum\limits_{j=1}^{n} w_{ij} \sum\limits_{i=1}^{n} (X_i - \overline{X})^2} \tag{7}$$

$$G_i^* = \frac{\sum\limits_{j=1}^{n} w_{ij}X_j - \overline{X} \sum\limits_{j=1}^{n} w_{ij}}{\sqrt{\frac{\sum\limits_{j=1}^{n} x_j^2}{n} - (\overline{X})^2} \sqrt{\frac{\left[n \sum\limits_{j=1}^{n} w^2{}_{ij} - \left(\sum\limits_{j=1}^{n} w_{ij}{}^2\right)\right]}{n-1}}} \tag{8}$$

where w_{ij} refers to the elements of spatial weight matrix, which represents the mutual spatial influence between subnational unit *i* and *j*. Here, we adopt queen contiguity matrix, which builds the neighborhood list based on edges or corners. The matrix element $w_{ij} = 1$ indicates that subnational unit *i* and *j* share an edge and/or a corner. Otherwise, $w_{ij} = 0$ indicates that subnational unit *i* and *j* do not share edges and/or corners; X_i and X_j are the $SHDI_{adjusted}$ value of the *i*th and *j*th subnational units in the spatial matrix, respectively; $\overline{X}$ refers to the average of $SHDI_{adjusted}$ of all subnational units; *n* is the total number of subnational units.

2.3.3. Trend Analysis (*Slope*)

To further clarify the overall trend of human development change in the Eastern Hemisphere during 1992–2013, we used a linear trend analysis method based on least squares to regress the time variables and HDI_{NTL} and expressed the magnitude of the changing trend by a *slope*. The trend analysis method was applied to the pixel level of HDI_{NTL} (i.e., $PHDI_{adjusted}$) to obtain the trend of $PHDI_{adjusted}$ over the whole study period, and thus visualizing the dynamics of the regional human development in the Eastern Hemisphere. The linear trend value (i.e., *slope*) was calculated as follows:

$$Slope = \frac{n \times \sum\limits_{i=1}^{n} t_i X_i - \sum\limits_{i=1}^{n} t_i \sum\limits_{i=1}^{n} X_i}{n \times \sum\limits_{i=1}^{n} t_i^2 - \left(\sum\limits_{i=1}^{n} t_i\right)^2} \tag{9}$$

where *n* refers to the time span, which is equal to 22 in this study; t_i refers to the *i*th year of the study period (1992 is the first year, 2013 is the 22nd year); X_i is the gridded level of HDI_{NTL} (i.e., $PHDI_{adjusted}$). A positive *slope* (*slope* > 0) indicates an upward trend, and a negative *slope* (*slope* < 0) represents a downward trend.

3. Results and Discussion

3.1. Performance Analysis of HDI_{NTL}

To verify the feasibility of constructing an income index with NTL instead of GNP, we examined the logarithmic correlation between NTL and GNP through scatter plots. As shown in Figure 3, NTL and GNP showed good positive correlations in all scatter plots. For instance, the NTL and GNP explained variation (R^2) was 0.706 in 1999 (Figure 3b), and the corresponding value reached 0.731 in 2013 (Figure 3d). There are a few outstanding data points with large residuals from the regression model. Some points circled with red dashed lines (e.g., East in North Macedonia) have a higher GNP than NTL DN value, which may be due to the saturation effect of the DMSP/OLS NTL data [46,47]. In addition, some subnational units, such as Kesk-Eesti in Estonia (circled with blue dashed lines), may be affected by the financial crisis or social instability, in significantly higher levels of NTL than GNP. Overall, the above results confirmed that NTL data have great potential for measuring GNP, and we can use it instead of GNP to construct the HDI_{NTL}.
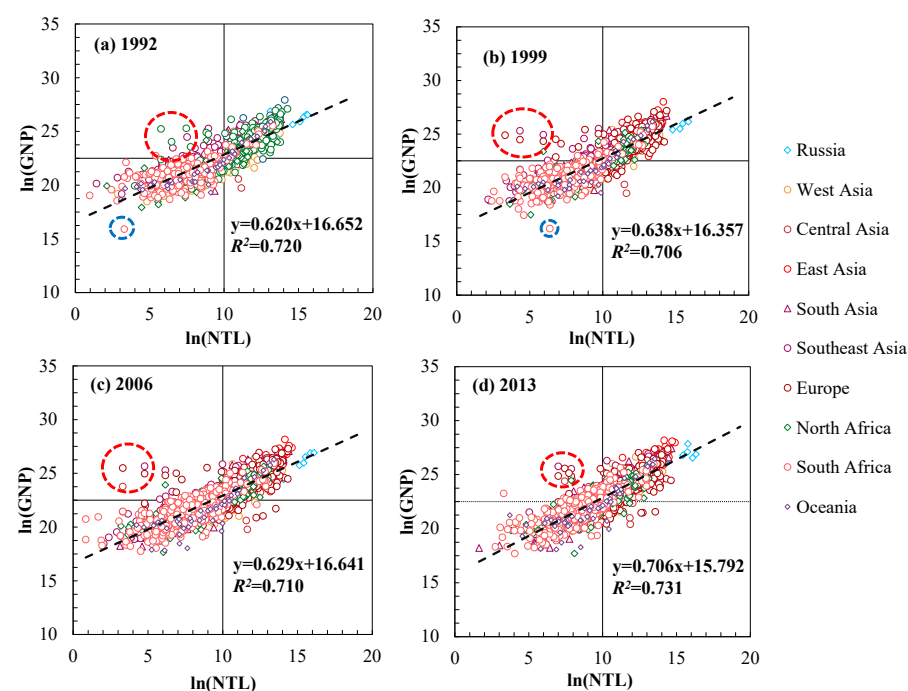

Figure 3. Loglog linear correlation between the total nighttime light (NTL) and gross national product (GNP) for each subnational unit in the Eastern Hemisphere in (**a**) 1992, (**b**) 1999, (**c**) 2006, and (**d**) 2013. Note that the different colored scatters are to distinguish the subnational units located in different regions.

We also compared the subnational HDI_{NTL} ($SHDI_{adjusted}$) with the SHDI data published by Smits and Permanyer [40] (Figure 4). The results showed that $SHDI_{adjusted}$ and SHDI had a significant linear relationship during 1992–2013, with R^2 reaching above 0.922. In particular, in 2013 (Figure 4d), there was a strong correlation between $SHDI_{adjusted}$ and SHDI, with an R^2 of 0.950. Thus, only in some individual subnational units, such as the East in North Macedonia (circled with red dashed lines), may be affected by the saturation effect of the DMSP/OLS NTL data, which results in $SHDI_{NTL}$ significantly lower than SHDI values. Overall, the $SHDI_{adjusted}$ was highly consistent with SHDI published by

Smits and Permanyer [40]. Therefore, our method of constructing HDI_{NTL} with NTL is feasible.
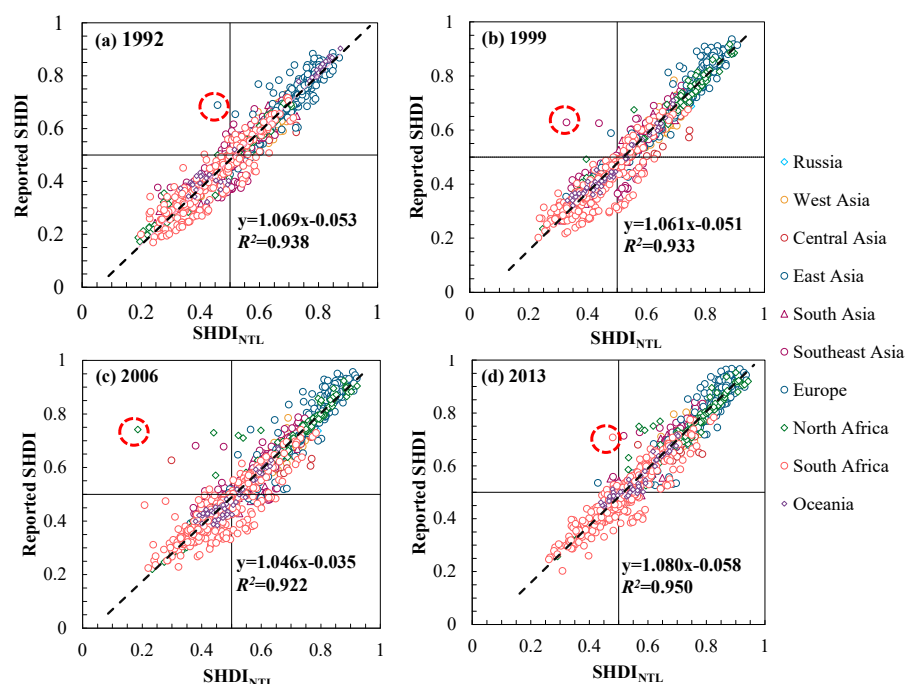

Figure 4. Correlation analysis between the subnational HDI_{NTL} ($SHDI_{NTL}$) and the reported Subnational Human Development Index (SHDI) in (**a**) 1992, (**b**) 1999, (**c**) 2006, and (**d**) 2013. Note that the reported SHDI refers to the data reported by the Subnational Human Development Database [40].

3.2. Spatiotemporal Analysis of HDI_{NTL} at the National Scale

3.2.1. Regional Disparity Analysis

We used the range analysis (maximum, mean, and minimum) to examine the discrepancies in $NHDI_{NTL}$ across regions in the Eastern Hemisphere (Figure 5). The $NHDI_{NTL}$ values ranged between 0.138 and 0.947 during 1992–2013. Overall, the smallest discrepancies in human development were observed among countries in Central Asia ($0.590 < NHDI_{NTL} < 0.786$), while the largest was found in North Africa ($0.188 < NHDI_{NTL} < 0.741$). The wide gap in human development among North African countries is directly related to their unbalanced economic development and educational development. For example, countries such as Somalia, Libya, and Sudan had a low overall quality of education and even more stagnant economic development due to war. Comparing the dynamics of $NHDI_{NTL}$ discrepancies, it was found that $NHDI_{NTL}$ discrepancies tend to decrease in most regions of Eastern Hemisphere, but there were still regions such as Central Asia where the discrepancies were getting larger.

Figures 5 and 6a showed the mean $NHDI_{NTL}$ values and their dynamics across nine geographic regions in the Eastern Hemisphere. The mean $NHDI_{NTL}$ in the Eastern Hemisphere regions ranged from 0.351 to 0.833. Comparing the mean $NHDI_{NTL}$ across regions in different years, the maximum and minimum values always occurred constantly in Europe and Sub-Saharan Africa, respectively. Except for North Africa and Oceania, which showed slight fluctuations in 1999, the average $NHDI_{NTL}$ in the other seven regions showed a steady upward trend. In particular, the mean $NHDI_{NTL}$ in Southeast Asia increased from 0.453 in 1992 to 0.612 in 2013.
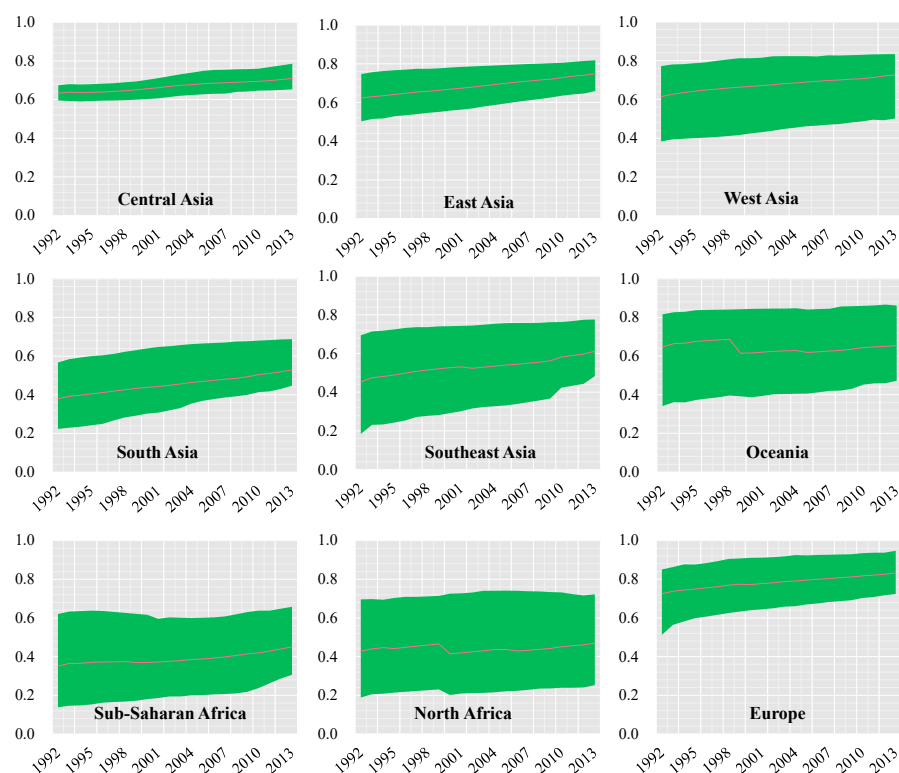
Figure 5. Range of the HDI$_{NTL}$ at national scale in the Eastern Hemisphere, 1992–2013. Note that the number on the y-axis represents the national HDI$_{NTL}$ value. The red line is the average of national HDI$_{NTL}$ for each region.
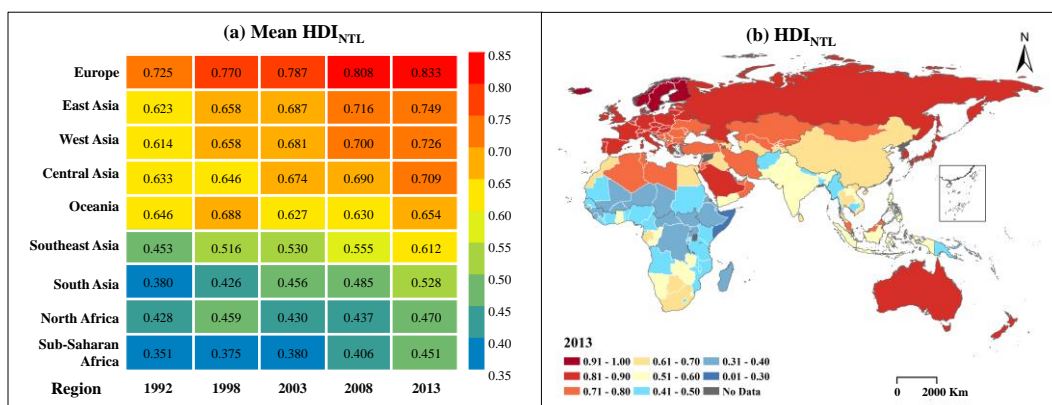

Figure 6. (**a**) The average value of HDI$_{NTL}$ at national scale in the Eastern Hemisphere, 1992–2013. (**b**) The spatial distribution map of HDI$_{NTL}$ at national scale in 2013.

Combining Figures 5 and 6a, we can have comprehensive knowledge of the magnitude and trend of NHDI$_{NTL}$ values in the Eastern Hemisphere, but the spatial distribution of NHDI$_{NTL}$ is not yet clear. Therefore, to further reveal the spatial disparity characteristics of each Eastern Hemisphere country, we displayed the NHDI$_{NTL}$ in 2013 in Figure 6b. Similar to the distribution trend of the mean NHDI$_{NTL}$ across regions, the countries with high NHDI$_{NTL}$ were concentrated in Europe, West Asia, and Oceania, while the countries with low NHDI$_{NTL}$ were in North Africa and Sub-Saharan Africa. The highest NHDI$_{NTL}$ was found in Finland (0.947), followed by Iceland (0.946) and Norway (0.945), and the lowest NHDI$_{NTL}$ was shown in Somalia (0.252). In terms of growth, Cambodia had the largest increase in NHDI at 0.313. It is worth noting that China has also made great progress in

human development over the past 22 years, with a significant increase in $NHDI_{NTL}$ values from 0.503 to 0.659.

3.2.2. Ranking Analysis

In general, $NHDI_{NTL}$ values are closely related to the level of socioeconomic development, that is countries with a high level of economic development also have a high $NHDI_{NTL}$ ranking. By comparing the $NHDI_{NTL}$ values and their rankings in five different years (i.e., 1992, 1998, 2003, 2008, and 2013), we found that six to seven countries consistently ranked in the top or bottom 10, respectively (Tables 3 and 4). The $NHDI_{NTL}$ values of the top 10 countries were nearly six times higher than those of the bottom 10 countries. In terms of the regions to which these countries belong, six consistently top 10 $NHDI_{NTL}$ countries were all concentrated in Europe (Table 3). Additionally, $NHDI_{NTL}$ values of these six countries also varied over time, but the ranking changes were not significant. The bottom 10 countries were concentrated in Sub-Saharan Africa (5/7) and North Africa (2/7) (Table 4). Although these countries' rankings did not improve significantly over the period 1992–2013, and in some cases even declined, the absolute value of $NHDI_{NTL}$ improved slightly for each country.

3.3. Spatiotemporal Analysis of HDI_{NTL} at the Subnational Scale

3.3.1. Spatial Clustering Analysis

Spatial autocorrelation analysis and hotspot analysis were conducted at the subnational scale to further explore the spatial patterns of human development in the Eastern Hemisphere. Results of spatial autocorrelation analysis showed moderate spatial clustering characteristics across different subnational units of Eastern Hemisphere during 1992–2013 (Table 5). According to the z-scores and *p*-values of significant tests, the spatial distribution of $SHDI_{NTL}$ was identified to follow a spatial clustering pattern. This meant that subnational units with high (or low) $SHDI_{NTL}$ values were most likely surrounded by surrounding subnational units with high (or low) $SHDI_{NTL}$ values. During the study period, Global Moran's I of $SHDI_{NTL}$ fluctuated slightly but showed an overall decreasing trend. That is, the spatial influence of geographically adjacent subnational units on each other's $SHDI_{NTL}$ became progressively weaker. It may indicate that economic and cultural exchanges between subnational units in the Eastern Hemisphere region broke through geographical constraints. Thus, the level of human development in the Eastern Hemisphere was spatially dependent, and there were extensive spatial linkages between them.

Table 3. Countries consistently ranked in the top 10 of HDI_{NTL} at national scale in the Eastern Hemisphere, 1992–2013. Note that there are 106 countries in Eastern Hemisphere with complete data.

Representative Countries	Region	1992		1998		2003		2008		2013	
		$NHDI_{NTL}$	Rank	$NHDI_{NTL}$	Rank	$NHDI_{NTL}$	Rank	$NHDI_{NTL}$	Rank	$NHDI_{NTL}$	Rank
Finland	Europe	0.819	3	0.870	3	0.897	3	0.924	2	0.947	1
Iceland	Europe	0.816	4	0.850	3	0.893	4	0.906	3	0.946	2
Norway	Europe	0.850	1	0.894	2	0.916	2	0.928	1	0.945	3
Sweden	Europe	0.833	2	0.905	1	0.918	1	0.904	4	0.935	4
Denmark	Europe	0.772	9	0.814	9	0.855	5	0.864	6	0.884	5
Belgium	Europe	0.798	6	0.836	5	0.847	7	0.858	7	0.866	8

Table 4. Countries consistently ranked in the bottom 10 of HDI$_{NTL}$ at national scale from 1992–2013. Note that there are 106 Eastern Hemisphere countries with complete data.

Representative Countries	Region	1992		1998		2003		2008		2013	
		NHDI$_{NTL}$	Rank	NHDI$_{NTL}$	Rank	NHDI$_{NTL}$	Rank	NHDI$_{NTL}$	Rank	NHDI$_{NTL}$	Rank
Central African Republic CAR	Sub-Saharan Africa	0.272	95	0.270	100	0.274	101	0.286	103	0.306	106
Burundi	Sub-Saharan Africa	0.180	103	0.215	105	0.231	105	0.269	104	0.313	105
Sierra Leone	Sub-Saharan Africa	0.138	105	0.168	106	0.194	106	0.210	106	0.315	104
Niger	North Africa	0.194	100	0.226	104	0.240	104	0.264	105	0.324	103
Mali	North Africa	0.188	101	0.248	101	0.295	100	0.333	100	0.359	102
Guinea	Sub-Saharan Africa	0.178	104	0.248	101	0.259	103	0.303	102	0.362	101
Rwanda	Sub-Saharan Africa	0.138	105	0.238	103	0.274	101	0.315	101	0.401	98

Table 5. Auto-spatial correlation of the HDI$_{NTL}$ at subnational scale in the Eastern Hemisphere, 1992–2013. Note that the number of asterisks (*) indicates different significance levels (*p*): 1 stands for $p < 0.05$, 2 stands for $p < 0.01$, 3 stands for $p < 0.001$. *C* represents the spatial clustering pattern, *D* represents the spatial disperse pattern, *R* represents the spatial random pattern.

Year	Moran's *I* Values	z-Score	*p*-Value	Pattern	Year	Moran's *I* Values	z-Score	*p*-Value	Pattern
1992	0.772	45.484	0.000 ***	*C*	2003	0.639	37.625	0.000 ***	*C*
1993	0.771	45.424	0.000 ***	*C*	2004	0.629	37.079	0.000 ***	*C*
1994	0.772	45.454	0.000 ***	*C*	2005	0.584	34.413	0.000 ***	*C*
1995	0.772	45.464	0.000 ***	*C*	2006	0.563	33.159	0.000 ***	*C*
1996	0.771	45.422	0.000 ***	*C*	2007	0.562	33.095	0.000 ***	*C*
1997	0.768	45.246	0.000 ***	*C*	2008	0.558	32.851	0.000 ***	*C*
1998	0.768	45.238	0.000 ***	*C*	2009	0.555	32.724	0.000 ***	*C*
1999	0.746	43.925	0.000 ***	*C*	2010	0.543	32.007	0.000 ***	*C*
2000	0.694	40.874	0.000 ***	*C*	2011	0.540	31.806	0.000 ***	*C*
2001	0.692	40.784	0.000 ***	*C*	2012	0.549	32.339	0.000 ***	*C*
2002	0.680	40.036	0.000 ***	*C*	2013	0.546	32.179	0.000 ***	*C*

Hotspot analysis allowed further exploration of the range of factors influencing autocorrelation between subnational units. Figure 7 showed the changes in the spatial distribution of different hot and cold spot units in SHDI$_{NTL}$ during 1992–2013. The hot spots units of SHDI$_{NTL}$ were mainly distributed in Europe, Russia, and Oceania (e.g., Finland, Belgium, Spain, Czech Republic, and Australia). Moreover, Sub-Saharan Africa countries had the largest proportion of cold spot clustering units in SHDI$_{NTL}$, while the number of cold spot units in SHDI$_{NTL}$ in this region was also increasing significantly. Moreover, the cold or hot spot units were further classified into three categories based on the significance of statistical hypothesis testing: 90% confidence level (i.e., $p < 0.1$), 95% confidence level (i.e., $p < 0.05$), and 99% confidence level (i.e., $p < 0.01$). The confidence level had increased significantly in some subnational units, such as the cold spot units of SHDI$_{NTL}$ in Congo and Angola.
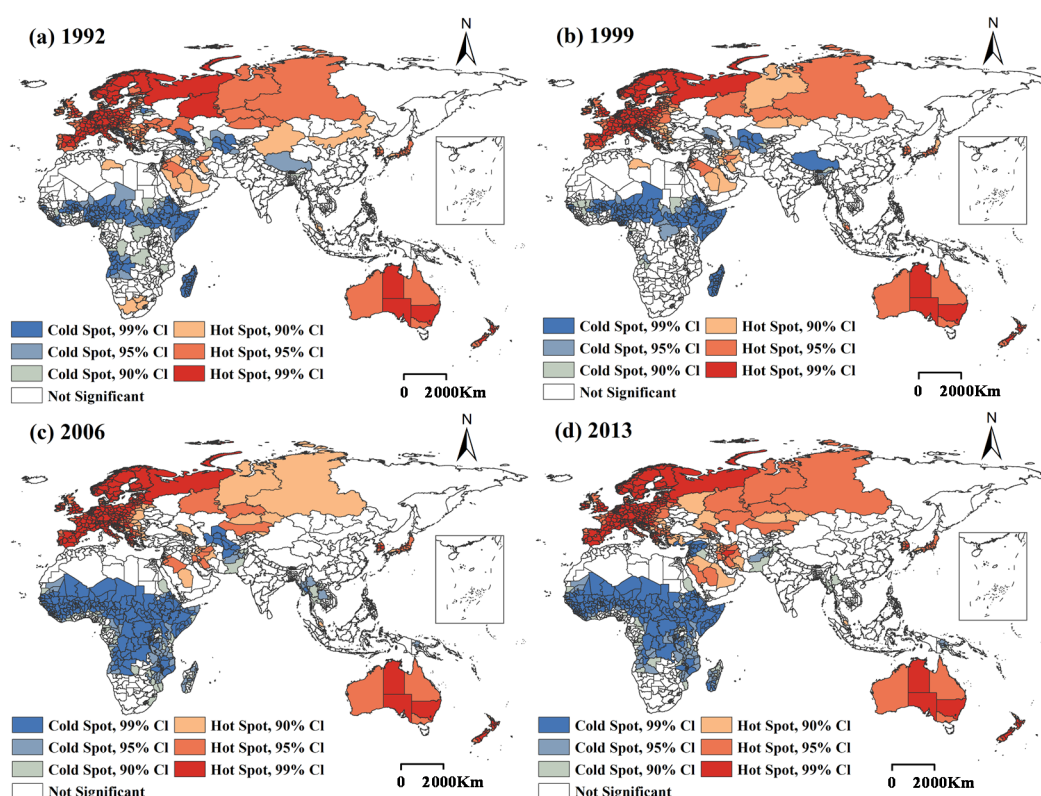
Figure 7. Hotspot analysis result (Getis-Ord G_i^* statistic) of HDI_{NTL} at subnational scale in the Eastern Hemisphere in (**a**) 1992, (**b**) 1999, (**c**) 2006, and (**d**) 2013.

3.3.2. Evolutionary Analysis

To further reveal the evolutionary characteristics of HDI_{NTL} in Eastern Hemisphere regions, we divided $SHDI_{NTL}$ values into four categories with reference to UNDP: 0–0.55 as low-level, 0.55–0.70 as medium-level, 0.70–0.80 as high-level, 0.80–1.0 as very high-level. As shown in Figure 8, the subnational units in the Eastern Hemisphere regions were at different human development levels. The subnational units with $SHDI_{NTL}$ at very high-level were concentrated in Europe and Oceania, while those at low-level were in Sub-Saharan Africa and South Asia. For instance, Norrland in northern Sweden had been at a very high level of human development ($SHDI_{NTL} > 0.84$) during 1992–2013, while southwestern Central African Republic had remained at a low level ($SHDI_{NTL} < 0.35$). Furthermore, $SHDI_{NTL}$ showed an obvious decreasing and then increasing trend along the northwest (i.e., subnational units in Europe) to southeast (i.e., subnational units in Oceania) direction of Eastern Hemisphere during the five points of the study period. From an overall evolutionary perspective, the Eastern Hemisphere subnational unit has seen a significant increase in the human development level. The percentage of subnational units with $SHDI_{NTL}$ at low-level and very high-level was 54.28% and 3.81%, respectively, in 1992. However, in 2013, the corresponding ratio evolved to 26.58% and 26.39%, respectively.

We also analyzed the evolutionary process of each subnational unit's human development levels throughout the study period. The evolutionary trajectories of the 1076 subnational units can be divided into three categories: (i) decrease type, in which the human development level in 2013 was lower than that in 1992, i.e., evolved from an upper level to a lower level; (ii) stable type, in which the human development level remained unchanged throughout the study period; (iii) increase type, which was the opposite of the decrease type, i.e., in which the human development level increased in a stepwise manner throughout the study period.

The proportions of subnational units with decrease type, stable type, and increase type of evolutionary trajectories were 0.65%, 38.38%, and 60.97%, respectively. Figure 9

showed the evolutionary trajectory of human development level for six representative subnational units. Different categories of subnational units had different evolutionary trajectories of human development levels, such as the evolutionary direction and inflection points. For instance, within the category of increase type, West Bengal of India soared from low-level to high-level in 2000, while this inflection point occurred much earlier in Tibet, China. The evolutionary trajectory from high-level to very high-level was relatively slow in both of these two subnational units. In general, however, the evolutionary trajectory of HDI_{NTL} in most subnational units was generally gradual, with few dramatic fluctuations in development levels.
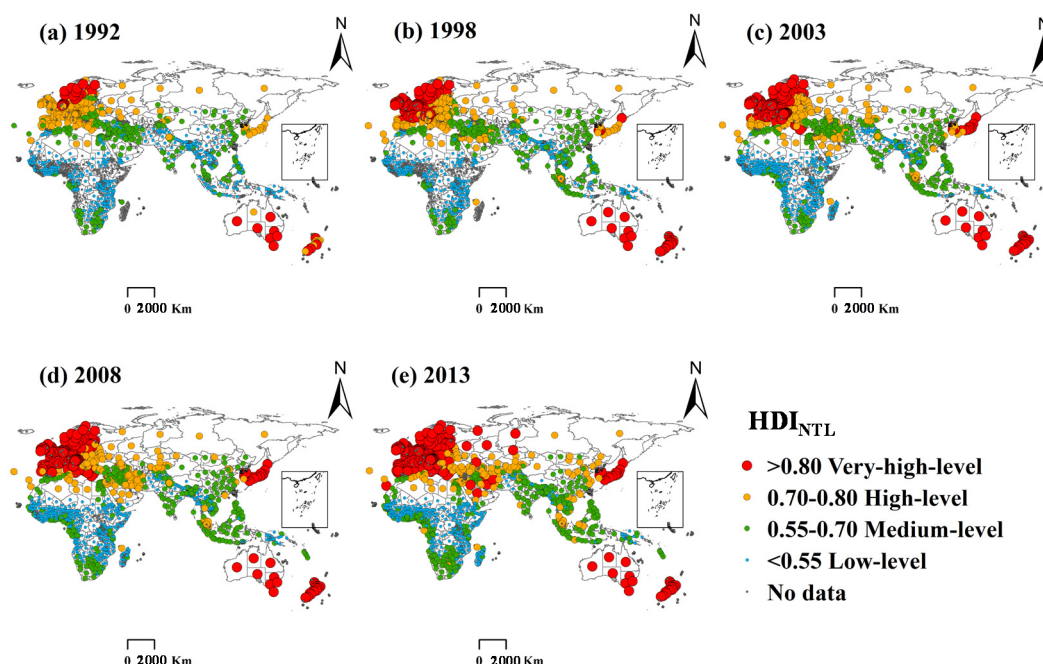
Figure 8. Categories of HDI_{NTL} at subnational scale in the Eastern Hemisphere in (**a**) 1992, (**b**) 1998, (**c**) 2003, (**d**) 2008, and (**e**) 2013. Note that there are 1076 subnational units for which $SHDI_{NTL}$ data are available.
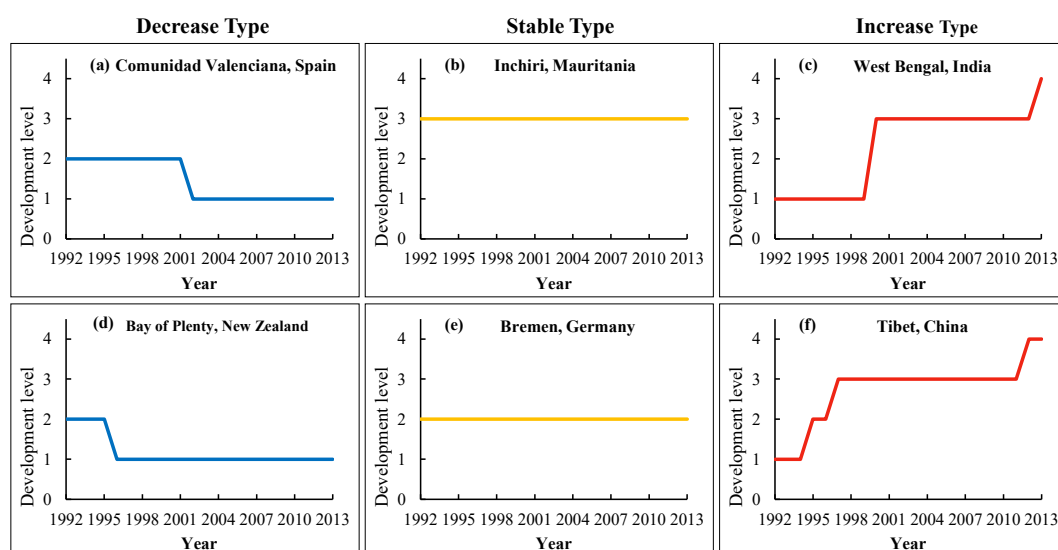
Figure 9. HDI_{NTL} evolution process at subnational scale in the Eastern Hemisphere, 1992–2013. Note that the number on the y-axis represents the human development level: 1 indicates the Low-level, 2 indicates the Medium-level, 3 indicates the High-level, and 4 indicates the Very-high-level.

3.4. Spatiotemporal Analysis of HDI$_{NTL}$ at the Pixel Scale

3.4.1. Spatial Variation Analysis

Figure 10 presents the gridded HDI$_{NTL}$ maps in 1992 and 2013 with a spatial resolution of 1 km, from which we can accurately compare the spatial pattern and regional disparities of human development in the Eastern Hemisphere. In 1992 (Figure 10a), the grids with high PHDI$_{NTL}$ values (shown in red) were gathered in Japan, Korea, and many European countries, while the grids with low PHDI$_{NTL}$ values (shown in blue) were concentrated in North African, Central Asian, South Asian, and Southeast Asian countries. By 2013 (Figure 10b), the high PHDI$_{NTL}$ gathering zone was significantly expanded, especially in eastern coastal areas and three urban agglomerations (i.e., Beijing-Tianjin-Hebei Region, Yangtze River Delta, Pearl River Delta) of China, where there was a significant increase in the pixel numbers of PHDI$_{NTL}$ larger than 0.5. Thus, the spatial pattern of PHDI$_{NTL}$ in the Eastern Hemisphere had changed over time.
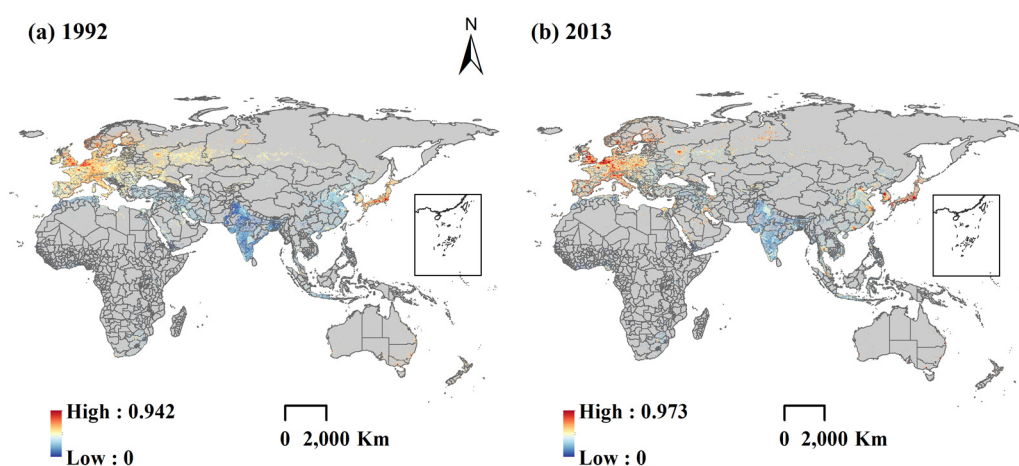
Figure 10. Spatial distribution map of HDI$_{NTL}$ at pixel scale in the Eastern Hemisphere in (**a**) 1992 and (**b**) 2013. Note that NoData areas are shown in gray.

Figure 11 illustrated the spatial map of pixel HDI$_{NTL}$ variations (ΔPHDI$_{NTL}$ = HDI$_{NTL2013}$ − HDI$_{NTL1992}$). Overall, many countries, including Pakistan, India, China, Saudi Arabia, Egypt, and Indonesia, showed substantial increases in PHDI$_{NTL}$ during the study period. For instance, Bohai Rim, Yangtze River Delta, and Pearl River Delta of China, these cities or regions had achieved remarkable growth in HDI$_{NTL}$ with relatively high ΔPHDI$_{NTL}$. The human development level of Bangalore, Madras, and Cochin of India also improved quickly in terms of ΔPHDI$_{NTL}$. The magnitude of PHDI$_{NTL}$ variations was very slight in European countries and regions, although they had higher absolute PHDI$_{NTL}$ values during 1992–2013. However, some cities or regions in Eastern Hemisphere were in the recession of PHDI$_{NTL}$, and ΔPHDI$_{NTL}$ was negative. For instance, Arlen and Luxembourg in Germany, Brno and Prague in the Czech Republic, and Ahvaz in northern Iran.
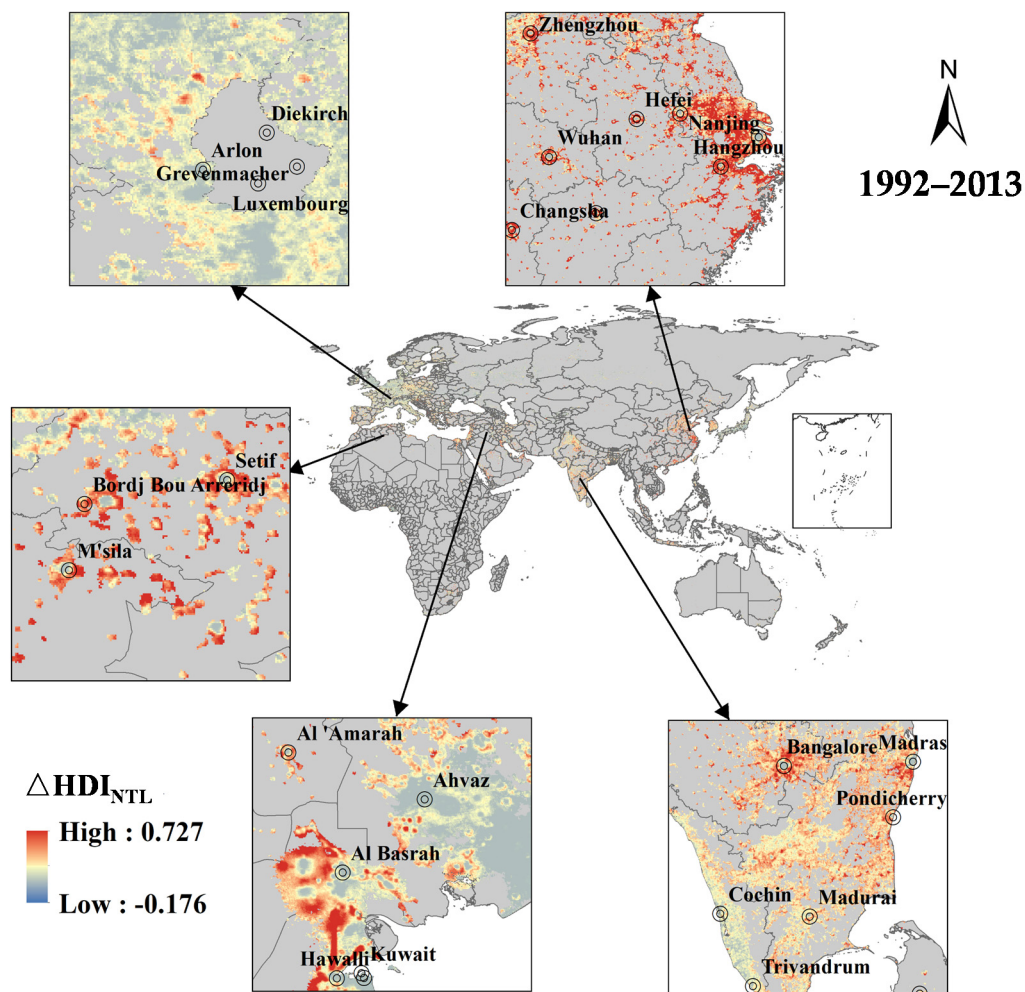
Figure 11. Spatial variation map of HDI$_{NTL}$ at pixel scale in the Eastern Hemisphere, 1992–2013. Note that the NoData areas are shown in gray.

3.4.2. Trend Analysis

Figure 12 showed the linear trend map of HDI$_{NTL}$ during 1992–2013 at a spatial resolution of 1 km in the Eastern Hemisphere regions. Overall, the growth trend of PHDI$_{NTL}$ in the Eastern Hemisphere region shows the characteristics that the slope in the northeast and southwest directions was significantly smaller than the central. Significantly, Europe in the northeast direction and Oceania in the southwest direction slope value is almost 0, which means that the PHDI$_{NTL}$ is almost no growth in these regions. In addition, the number of pixels with PHDI$_{NTL}$ slope value greater than 0 was 663244, accounting for 93.52%, which indicates that the HDI in the region is dominated by the rapid growth type and the level of human development has been significantly improved. Additionally, these HDI$_{NTL}$ fast-growing grids were mainly distributed in East Asia, West and South Asia.
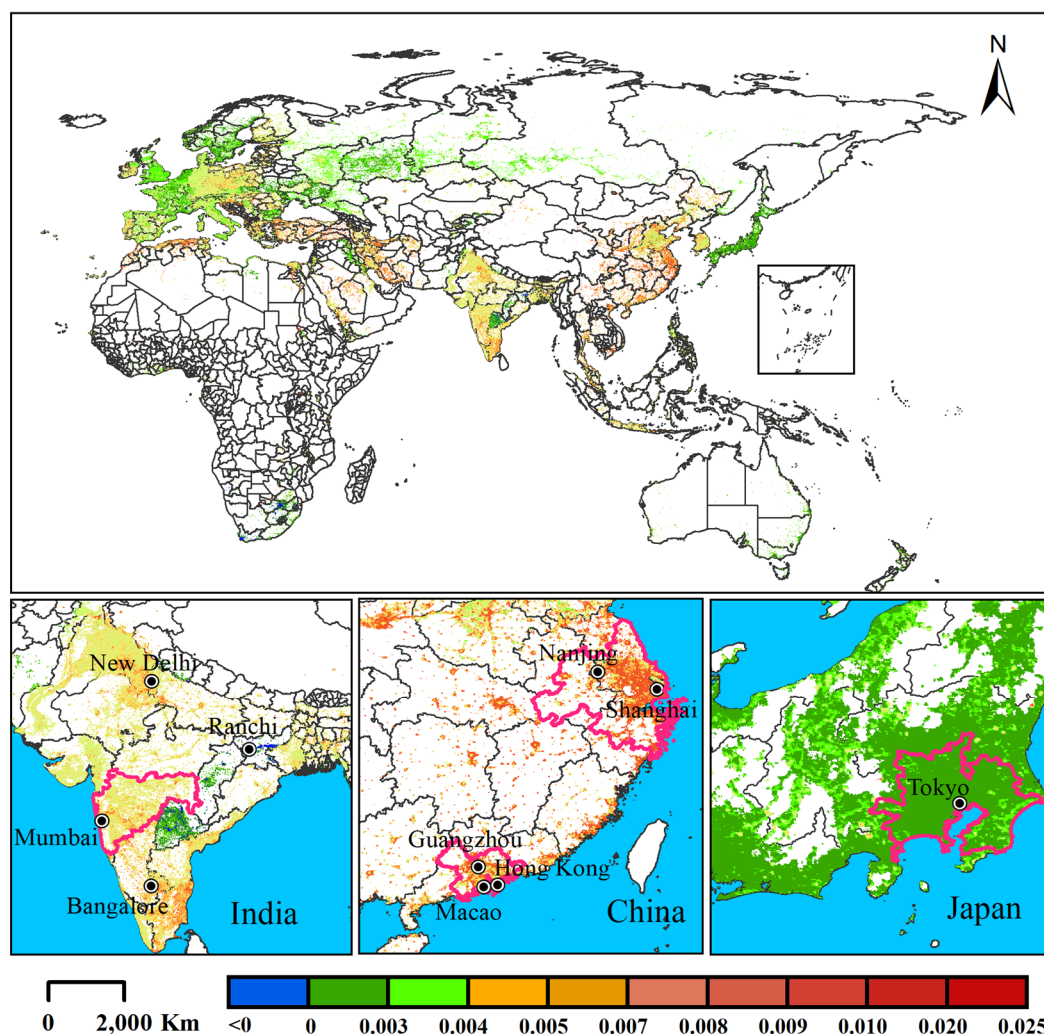
Figure 12. Evolutionary trend of HDI$_{NTL}$ at pixel scale in the Eastern Hemisphere, 1992–2013. Note that the bottom three maps highlight four representative urban agglomerations in pink. From left to right, they are Mumbai Urban Agglomerations in India, Guangdong-Hong Kong-Macao Greater Bay Area and Yangtze River Delta Urban Agglomerations in China, Tokyo Metropolitan Area in Japan. NoData areas are shown in white.

We also selected India, China, and Japan to analyze the evolutionary characteristics of HDI$_{NTL}$ within these countries specifically. The evolutionary trend of HDI$_{NTL}$ varied widely within India, with significant growth zones (e.g., New Delhi, Mumbai, and Bangalore) and decline zones (Ranchi). In China, which is also a developing country, there was no downward trend in HDI$_{NTL}$. Moreover, China's large urban agglomerations, such as the Yangtze River Delta and the Guangdong-Hong Kong-Macao Greater Bay Area, were experiencing impressive HDI$_{NTL}$ growth. Unlike China and India, Japan's HDI$_{NTL}$ was not declining during 1992–2013, but its growth rate was very slow.

4. Conclusions and Policy Implications

4.1. Conclusions

In this paper, we developed the new HDI$_{NTL}$ by retaining the structure and logic of the traditional HDI and using NTL data to reconstruct the income index. It enables an efficient and timely assessment of human development status at finer spatial resolutions. Through the application of HDI$_{NTL}$ at the multiple scales (i.e., national, subnational, and pixel scales) of the Eastern Hemisphere regions during 1992–2013, the human development status and its spatiotemporal dynamics of the Eastern Hemisphere region were investigated. The major conclusions are summarized as follows.

(1) The linear regression analysis suggests that NTL had a significant correlation with GNP (R^2 > 0.706). The $SHDI_{NTL}$ also correlated with the reported SHDI (R^2 > 0.922), which suggested that HDI_{NTL} could measure the human development level of the Eastern Hemisphere regions with high validity.

(2) At the national scale, the smallest discrepancies in human development were observed among countries in Central Asia (0.590 < HDI_{NTL} < 0.786), while the largest was in North Africa (0.188 < HDI_{NTL} < 0.741). The six consistently ranked top 10 $NHDI_{NTL}$ countries were all concentrated in Europe, while the seven consistently ranked bottom 10 countries were in Sub-Saharan Africa and North Africa.

(3) At the subnational scale, HDI_{NTL} showed an obvious decreasing and then increasing trend along the northwest (i.e., subnational units in Europe) to southeast (i.e., subnational units in Oceania) direction of Eastern Hemisphere. The spatial distribution of the HDI_{NTL} showed a clear clustering feature based on the results of global Moran's *I* and hotspot analysis. The evolutionary trajectories of HDI_{NTL} were classified into three types (i.e., decrease type, stable type, and increase type), with the increase type of subnational units accounting for the largest proportion.

(4) At pixel scale, the spatial distribution of the high HDI_{NTL} zones and low HDI_{NTL} zones had prominent agglomeration characteristics. The evolutionary trend of HDI_{NTL} was dominated by the fast-growing type during 1992–2013, with 93.52% of the grids with slope values greater than 0. Large urban agglomerations in India and China were leading the way in terms of HDI_{NTL} growth.

4.2. Policy Implications

Achieving the coordinated development of health, education and economic dimensions at the national level is essential for improving human well-being as well as promoting global sustainable development. This study gives a picture of human development at multiple scales (i.e., national, subnational, pixel scales), facilitating researchers, policy makers, and others to compare the current status and trends of human development in Eastern Hemisphere countries. Additionally, some policy recommendations are discussed to reduce the disparity in human development levels between countries and to promote the improvement of human development levels in the Eastern Hemisphere.

(1) Reducing human development disparities among countries in the Eastern Hemisphere is a challenging but essential task. It requires countries to adopt sound human development policies to support this comprehensive development pattern, especially the most relevant economic, education, and health policies. Countries and regions at higher levels of human development should work closely with those at lower levels (e.g., Southeast Asia and South Asia), providing financial and technical support to promote their economic development. Besides, all geographical units should recognize the importance of rational allocation of resources and promote the rational flow of production factors to achieve balanced and sustainable development.

(2) The educated population and education level of a country or region will constrain future economic growth and significantly affect cultural exchanges between countries or regions, thus affecting human development. Therefore, Eastern Hemisphere regions and countries should increase investment in primary education, improve the labor force's quality, and develop high-tech industries while carrying out cultural exchanges and educational cooperation to strengthen the interaction of talents between regions.

(3) Although countries with high (or low) HDI_{NTL} were spatially clustered, some countries with high HDI_{NTL} values were still mixed with low HDI_{NTL} countries. Countries with high HDI_{NTL} generally have distinct advantages, e.g., better economic base, higher labor education level, and longer average life expectancy. Therefore, these high-HDI_{NTL} countries can play the role of growth poles and expand the scope of economic cooperation to provide more development opportunities for low HDI_{NTL} countries, thus achieving a balance of human development in the Eastern Hemisphere regions.

Yet, this paper also has some limitations that can be further improved in future work. The Defense Meteorological Satellite Program's Operational Linescan System (DMSP-OLS) NTL data we used has the limited coverage year of 1992–2013, and the spatial resolution is relatively low (~1 km). Since 2013, the new version of NTL supplied by the Suomi-National Polar-orbiting Partnership Visible Infrared Imaging Radiometer Suite (S-NPP VIIRS) satellite has been provided a higher spatial resolution (~500 m) and more precise observation. The S-NPP NTL product can be used to model socioeconomic indicators [48,49]. In the follow-up study, we plan to use S-NPP VIIRS NTL data as a proxy to reconstruct HDI, aiming to analyze the human development status after the year 2013 with finer spatial details.

Finally, another future concern is to carry out integrated research with the improved HDI accounting method. NTL data is good complementary consumption-based information for highlighting the socioeconomic hotspots areas, hereby with high potential to be integrated with environmental, physical, and socioeconomic data, to analyze the sustainability issues in a broader scope (e.g., incorporating carbon footprint and other environmental footprint indicators), and bridge the boundaries of general geography (location and land use perspective), metabolic geography (e.g., consumption-based material and energy metabolism), as well as human geography (socioeconomic activities as the carrier of material and energy flow), so as to help to quantify the interaction of social metabolism agents and the drivers to consumption.

Abbreviation

Abbreviations	Full Names
DMSP/OLS	The Defense Meteorological Satellite Program's Operational Linescan System
DN	Digital number values of nighttime lights
$DN_{adjusted}$	Adjusted digital number values of nighttime lights
GNP	Gross national product
HDI	Human Development Index
HDI_{NTL}	New Human Development Index reconstructed using nighttime lights
$NHDI_{NTL}$	The national HDI_{NTL}
$\Delta PHDI_{NTL}$	The HDI_{NTL} change value at each pixel during 1992–2013
$PHDI_{NTL1992}$	The HDI_{NTL} value at each pixel in 1992
$PHDI_{NTL2013}$	The HDI_{NTL} value at each pixel in 2013
$I_{education}$	Education Index
I_{Health}	Health Index
I_{NTL}	NTL Index, the index calculated by nighttime lights data
NOAA/NGDC	National Oceanic and Atmospheric Administration's National Geophysical Data Center
NLDI	Night light development index
NTL	Nighttime lights
ORNL	the Department of Energy's Oak Ridge National Laboratory
$PHDI_{NTL}$	The HDI_{NTL} at pixel level
$PHDI_{adjusted}$	The adjusted HDI_{NTL} at pixel level
$\Delta PHDI_{NTL}$	The HDI_{NTL} change value at each pixel during 1992–2013
$PHDI_{NTL1992}$	The HDI_{NTL} value at each pixel in 1992
$PHDI_{NTL2013}$	The HDI_{NTL} value at each pixel in 2013
SDGs	Sustainable development goals
SHDI	The data published by Subnational Human Development Database
$SHDI_{NTL}$	The HDI_{NTL} at subnational level
$SHDI_{adjusted}$	The adjusted HDI_{NTL} at subnational level
S-NPP VIIRS	Suomi-National Polar-orbiting Partnership
UNDP	United Nations Development Programme

References

1. Jing, C.; Tao, H.; Jiang, T.; Wang, Y.; Zhai, J.; Cao, L.; Su, B. Population, urbanization and economic scenarios over the Belt and Road region under the Shared Socioeconomic Pathways. *J. Geogr. Sci.* **2020**, *30*, 68–84. [CrossRef]
2. Malik, K. Human Development Report 2013. The Rise of the South: Human Progress in a Diverse World (15 March 2013). UNDP-HDRO Human Development Reports. 2013. Available online: https://ssrn.com/abstract=2294673 (accessed on 14 June 2021).
3. Martínez-Guido, S.I.; González-Campos, J.B.; Ponce-Ortega, J.M. Strategic planning to improve the Human Development Index in disenfranchised communities through satisfying food, water and energy needs. *Food Bioprod. Process.* **2019**, *117*, 14–29. [CrossRef]
4. Biggeri, M.; Mauro, V. Towards a more 'sustainable' human development index: Integrating the environment and freedom. *Ecol. Indicat.* **2018**, *91*, 220–231. [CrossRef]
5. Ladi, T.; Mahmoudpour, A.; Sharifi, A. Assessing impacts of the water poverty index components on the human development index in Iran. *Habitat Int.* **2021**, *113*, 102375. [CrossRef]
6. Donohue, C.; Biggs, E. Monitoring socio-environmental change for sustainable development: Developing a Multidimensional Livelihoods Index (MLI). *Appl. Geogr.* **2015**, *62*, 391–403. [CrossRef]
7. Dervis, K.; Klugman, J. Measuring human progress: The contribution of the Human Development Index and related indices. *Rev. D'écon. Polit.* **2011**, *121*, 73–92. [CrossRef]
8. Spangenberg, J.H. The Corporate Human Development Index CHDI: A tool for corporate social sustainability management and reporting. *J. Clean. Prod.* **2016**, *134*, 414–424. [CrossRef]
9. Neumayer, E. The human development index and sustainability—A constructive proposal. *Ecol. Econ.* **2001**, *39*, 101–114. [CrossRef]
10. Klugman, J.; Rodríguez, F.; Choi, H.J. The HDI 2010: New controversies, old critiques. *J. Econ. Inequal.* **2011**, *9*, 249–288. [CrossRef]
11. Sanusi, Y.A. Application of human development index to measurement of deprivations among urban households in Minna, Nigeria. *Habitat Int.* **2008**, *32*, 384–398. [CrossRef]
12. Tian, Q.; Brown, D.G.; Bao, S.; Qi, S. Assessing and mapping human well-being for sustainable development amid flood hazards: Poyang Lake Region of China. *Appl. Geogr.* **2015**, *63*, 66–76. [CrossRef]

13. Wang, Z.; Danish; Zhang, B.; Wang, B. Renewable energy consumption, economic growth and human development index in Pakistan: Evidence form simultaneous equation model. *J. Clean. Prod.* **2018**, *184*, 1081–1090. [CrossRef]

14. Kummu, M.; Taka, M.; Guillaume, J.H.A. Gridded global datasets for gross domestic product and human development index over 1990–2015. *Sci. Data* **2018**, *5*, 180004. [CrossRef] [PubMed]

15. Ji, X.; Li, X.; He, Y.; Liu, X. A simple method to improve estimates of county-level economics in China using nighttime light data and GDP growth rate. *ISPRS Int. J. Geo-Inf.* **2019**, *8*, 419. [CrossRef]

16. Yee, S.H.; Paulukonis, E.; Buck, K.D. Downscaling a human well-being index for environmental management and environmental justice applications in Puerto Rico. *Appl. Geogr.* **2020**, *123*, 102231. [CrossRef]

17. Jing, X.; Yan, Y.Z.; Yan, L.; Zhao, H. A novel method for saturation effect calibration of DMSP/OLS stable light product based on GDP grid data in China mainland at city level. *Geogr. Geo Inf. Sci.* **2017**, *33*, 35–39.

18. Tan, M.; Li, X.; Li, S.; Xin, L.; Wang, X.; Li, Q.; Li, W.; Li, Y.; Xiang, W. Modeling population density based on nighttime light images and land use data in China. *Appl. Geogr.* **2018**, *90*, 239–247. [CrossRef]

19. Li, X.; Zhou, W. Dasymetric mapping of urban population in China based on radiance corrected DMSP-OLS nighttime light and land cover data. *Sci. Total Environ.* **2018**, *643*, 1248–1256. [CrossRef]

20. Ye, T.; Zhao, N.; Yang, X.; Ouyang, Z.; Liu, X.; Chen, Q.; Hu, K.; Yue, W.; Qi, J.; Li, Z.; et al. Improved population mapping for China using remotely sensed and points-of-interest data within a random forests model. *Sci. Total Environ.* **2019**, *658*, 936–946. [CrossRef]

21. Dai, Z.; Hu, Y.; Zhao, G. The suitability of different nighttime light data for GDP estimation at different spatial scales and regional levels. *Sustainability* **2017**, *9*, 305. [CrossRef]

22. Zhao, N.; Cao, G.; Zhang, W.; Samson, E.L. Tweets or nighttime lights: Comparison for preeminence in estimating socioeconomic factors. *ISPRS J. Photogramm. Remote Sens.* **2018**, *146*, 1–10. [CrossRef]

23. Liang, H.; Guo, Z.; Wu, J.; Chen, Z. GDP spatialization in Ningbo City based on NPP/VIIRS night-time light and auxiliary data using random forest regression. *Adv. Space Res.* **2020**, *65*, 481–493. [CrossRef]

24. Mellander, C.; Lobo, J.; Stolarick, K.; Matheson, Z. Night-time light data: A good proxy measure for economic activity? *PLoS ONE* **2015**, *10*, e0139779. [CrossRef] [PubMed]

25. Jasiński, T. Modeling electricity consumption using nighttime light images and artificial neural networks. *Energy* **2019**, *179*, 831–842. [CrossRef]

26. Cao, X.; Wang, J.; Chen, J.; Shi, F. Spatialization of electricity consumption of China using saturation-corrected DMSP-OLS data. *Int. J. Appl. Earth Obs. Geoinf.* **2014**, *28*, 193–200. [CrossRef]

27. Dai, E.; Wang, Y. Attribution analysis for water yield service based on the geographical detector method: A case study of the Hengduan Mountain region. *J. Geogr. Sci.* **2020**, *30*, 1005–1020. [CrossRef]

28. Liang, H.; Tanikawa, H.; Matsuno, Y.; Dong, L. Modeling in-use steel stock in China's buildings and civil engineering infrastructure using time-series of DMSP/OLS nighttime lights. *Remote Sens.* **2014**, *6*, 4780–4800. [CrossRef]

29. Liang, H.; Dong, L.; Tanikawa, H.; Zhang, N.; Gao, Z.; Luo, X. Feasibility of a new-generation nighttime light data for estimating in-use steel stock of buildings and civil engineering infrastructures. *Resour. Conserv. Recycl.* **2017**, *123*, 11–23. [CrossRef]

30. Beyer, R.C.; Franco-Bedoya, S.; Galdo, V. Examining the economic impact of COVID-19 in India through daily electricity consumption and nighttime light intensity. *World Dev.* **2021**, *140*, 105287. [CrossRef]

31. Levin, N.; Duke, Y. High spatial resolution night-time light images for demographic and socio-economic studies. *Remote Sens. Environ.* **2012**, *119*, 1–10. [CrossRef]

32. Zhang, G.; Guo, X.; Li, D.; Jiang, B. Evaluating the potential of LJ1-01 nighttime light data for modeling socio-economic parameters. *Sensors* **2019**, *19*, 1465. [CrossRef]

33. Gao, B.; Huang, Q.; He, C.; Dou, Y. Similarities and differences of city-size distributions in three main urban agglomerations of China from 1992 to 2015: A comparative study based on nighttime light data. *J. Geogr. Sci.* **2017**, *27*, 533–545. [CrossRef]

34. Elvidge, C.D.; Baugh, K.E.; Anderson, S.; Sutton, P.; Ghosh, T. The Night Light Development Index (NLDI): A spatially explicit measure of human development from satellite data. *Soc. Geogr.* **2012**, *7*, 23–35. [CrossRef]

35. Wu, J.; Wang, Z.; Li, W.; Peng, J. Exploring factors affecting the relationship between light consumption and GDP based on DMSP/OLS nighttime satellite imagery. *Remote Sens. Environ.* **2013**, *134*, 111–119. [CrossRef]

36. He, C.; Ma, Q.; Liu, Z.; Zhang, Q. Modeling the spatiotemporal dynamics of electric power consumption in Mainland China using saturation-corrected DMSP/OLS nighttime stable light data. *Int. J. Digit. Earth* **2013**, *7*, 993–1014. [CrossRef]

37. Zhao, M.; Cheng, W.; Zhou, C.; Li, M.; Wang, N.; Liu, Q. GDP spatialization and economic differences in south china based on NPP-VIIRS nighttime light imagery. *Remote Sens.* **2017**, *9*, 673. [CrossRef]

38. National Remote Sensing Center of China (GEOARC). Global Ecosystems and Environment Observation Analysis Research Cooperation: The Belt and Road Initiative Ecological and Environmental Conditions. 2017. Available online: http://www.chinageoss.cn/geoarc/2017/pdf/ydyl2017_en.pdf (accessed on 14 June 2021).

39. Herrmann, S.M.; Mohr, K.I. A continental-scale classification of rainfall seasonality regimes in africa based on gridded precipitation and land surface temperature products. *J. Appl. Meteorol. Clim.* **2011**, *50*, 2504–2513. [CrossRef]

40. Smits, J.; Permanyer, I. The subnational human development database. *Sci. Data* **2019**, *6*, 190038. [CrossRef]

41. Goldewijk, K.K.; Beusen, A.; Janssen, P. Long-term dynamic modeling of global population and built-up area in a spatially explicit way: HYDE 3.1. *Holocene* **2010**, *20*, 565–573. [CrossRef]

42. Elvidge, C.D.; Ziskin, D.; Baugh, K.E.; Tuttle, B.T.; Ghosh, T.; Pack, D.W.; Erwin, E.H.; Zhizhin, M. A fifteen year record of global natural gas flaring derived from satellite data. *Energies* **2009**, *2*, 595–622. [CrossRef]

43. Boots, B.; Tiefelsdorf, M. Global and local spatial autocorrelation in bounded regular tessellations. *J. Geogr. Syst.* **2000**, *2*, 319–348. [CrossRef]

44. Hong, L.; Liang, N.; Di, W. Economic and environmental gains of China's fossil energy subsidies reform: A rebound effect case study with EIMO model. *Energy Policy* **2013**, *54*, 335–342. [CrossRef]

45. Xu, H.; Demetriades, A.; Reimann, C.; Jiménez, J.J.; Filser, J.; Zhang, C. Identification of the co-existence of low total organic carbon contents and low pH values in agricultural soil in north-central Europe using hot spot analysis based on GEMAS project data. *Sci. Total Environ.* **2019**, *678*, 94–104. [CrossRef]

46. Elvidge, C.D.; Baugh, K.E.; Dietz, J.B.; Bland, T.; Sutton, P.; Kroehl, H.W. Radiance calibration of DMSP-OLS low-light imaging data of human settlements. *Remote Sens. Environ.* **1999**, *68*, 77–88. [CrossRef]

47. Letu, H.; Hara, M.; Tana, G.; Nishio, F. A saturated light correction method for DMSP/OLS nighttime satellite imagery. *IEEE Trans. Geosci. Remote Sens.* **2012**, *50*, 389–396. [CrossRef]

48. Sahoo, S.; Gupta, P.K.; Srivastav, S.K. Comparative analysis between VIIRS-DNB and DMSP-OLS night-time light data to estimate electric power consumption in Uttar Pradesh, India. *Int. J. Remote Sens.* **2019**, *41*, 2565–2580. [CrossRef]

49. Shi, K.F.; Yu, B.L.; Huang, Y.X.; Hu, Y.J.; Yin, B.; Chen, Z.Q.; Chen, L.J.; Wu, J.P. Evaluating the ability of npp-viirs nighttime light data to estimate the gross domestic product and the electric power consumption of China at multiple scales: A comparison with DMSP-OLS Data. *Remote Sens.* **2014**, *6*, 1705–1724. [CrossRef]